LAWRENCE
LIVERMORE
NATIONAL
LABORATORY

# High-Temperature Studies of Glass Dissolution Rates Close to Saturation

*M. Zavarin, S.K. Roberts, P. Zhao, R.W. Williams,T.P. Rose, A. Rainer, and G.A. Pawloski*

**February 2004**

# High-Temperature Studies of Glass Dissolution Rates
## Close to Saturation

Mavrik Zavarin[1], Sarah K. Roberts[1], Pihong Zhao[2], Ross W. Williams[2],
Timothy P. Rose[2], Amanda Rainer[1], and Gayle A. Pawloski[1]

[1]Geosciences and Environmental Technologies Division,
Energy and Environment Directorate

[2]Chemical Biology and Nuclear Science Division,
Chemistry & Material Sciences Directorate

Lawrence Livermore National Laboratory
Livermore, California

Final Report
February 1, 2004

**TABLE OF CONTENTS**

# LIST OF FIGURES

# LIST OF TABLES

# 1    INTRODUCTION

Most long-lived radionuclides associated with an underground nuclear test are incorporated into a melt glass and are released by glass dissolution to become part of the hydrologic source term (HST) (Pawloski et al., 2001).  Although the rates of rhyolite glass dissolution are well known under conditions where the fluid is far from saturation with respect to glass, the rates are not well known under conditions where the fluid approaches saturation.  These rates are commonly much lower than the far-from-saturation rates, often by a factor greater than 100.  In recent HST simulations (Pawloski et al., 2001; Pawloski et al., 2000; Tompson et al., 1999), we conservatively estimated steady-state release rates based on a far-from-saturation fluid conditions.  In recent CHESHIRE near-field simulations (Pawloski et al., 2001), it was predicted that ~30% of the nuclear melt glass dissolved over 1000 years.  Although the "far-from-saturation rate" approach provides a conservative estimate of glass dissolution, it may greatly overestimate the rates of melt glass dissolution.  At CHESHIRE, less conservative estimates suggest that only ~1% of the nuclear melt glass will dissolve in 1000 years.  Lower glass dissolution rates result in lower radionuclide release rates from nuclear melt glass.  The following report documents glass dissolution experiments performed to measure glass dissolution rates close to saturation.

We performed a set of glass dissolution rate measurements using single-pass flow-through (SPFT) reactors.  Fluid saturation with respect to glass was controlled by adjusting the rate of fluid flow through a "pre-reactor" column packed with high-surface-area analog nuclear melt glass.  The fluid was then passed through a second reactor column with Mo-doped glass.  A key aspect of these experiments was to incorporate a small amount of molybdenum in the reator glass to use as a measure of glass dissolution rate.  This technique has been used successfully to measure rates of dissolution of extremely slowly reacting ceramics.  Glass dissolution experiments were performed at constrained pH values, saturation states, and temperatures (40 to 80ºC).  In addition to SPFT experiments, a batch dissolution experiment was performed at 160ºC to evaluate dissolution rates at higher temperatures.  Carle et al. (2003) described the impact of nuclear test heat on groundwater flow.  Their work suggests that resaturation of the melt glass zone may occur at temperatures as high as 250°C.  Thus, the range of temperatures examined in these experiments covers much of the anticipated range for Nevada Test Site (NTS) nuclear melt glass dissolution temperatures.[1]  Our glass dissolution data are compared with glass dissolution model predictions in Pawloski et al. (2001).  Based on these data, adjusted glass dissolution model parameters are recommended.

In a parallel set of experiments, SPFT tests were performed with real nuclear melt glass from the NTS.  These investigations used the same experimental protocol as analog experiments. However, due to extensive E&SH requirements using radioactive samples at high temperatures/pressures, nuclear melt glass samples were examined only to 80˚C.

---

[1] Prior to nuclear melt glass resaturation, glass dissolution would not occur since water is required for glass to dissolve.

Comparison of nuclear melt glass and analog glass results is used to validate our hypothesis that dissolution rates of nuclear melt glasses should be equivalent to non-radioactive analog glasses. The successful comparisons may make it operationally easier and technically defensible to use analogs instead of nuclear melt glasses in any future experiments as well as to validate the transfer of published analog glass data to nuclear melt glass dissolution models.

## 2 BACKGROUND

The glass dissolution model used in HST modeling at CHESHIRE (Pawloski et al., 2001) is based on the transition state theory (TST). Glass dissolution is defined by an equation of the following form:

$$r = k_0 \times e^{\frac{E_a}{R}\left(\frac{T-T_0}{T_0 T}\right)} \times A_s \times \prod_i a_i^{n_i} \times \left(1 - \left(\frac{Q}{K}\right)^{\frac{1}{\sigma}}\right)^{\upsilon} + A_s k_f \qquad (1)$$

where $r$ is the rate of glass dissolution (mol-glass g$^{-1}$ sec$^{-1}$), $k_0$ is the far-from-saturation glass dissolution rate (mol-glass m$^{-2}$ sec$^{-1}$) at temperature $T_0$, $E_a$ is the activation energy (cal mol$^{-1}$) which accounts for the change in glass dissolution as a function of temperature, $R$ is the gas constant (1.99 cal mol$^{-1}$ K$^{-1}$), $T$ and $T_0$ are the temperature of interest and the reference temperature (typically 25°C), respectively, $A_s$ is the surface area of the glass (m$^2$ g$^{-1}$), $a_i^n$ are a series of dissolution-inhibiting or -promoting solution aqueous species activities taken to some exponent $n$, $Q$ is the saturation of the solution relative to the solubility product of the glass ($K$). The term $\sigma$ is related, in TST, to the stoichiometry of the rate limiting reaction step but is generally fitted empirically. The term $\upsilon$ is an empirical term often added to the dissolution/precipitation model. Finally, $k_f$ is the close-to-saturation term (mol-glass g$^{-1}$ sec$^{-1}$), which is included to account for dissolution very close to saturation. In the following text, we describe how the various terms in the glass dissolution equation affect glass dissolution as a function of solution and solid composition.

The far-from-saturation glass dissolution rate, $k_0$, has been well documented in the literature for silicate glasses. Our glass dissolution model was based upon measurements by Mazer (1987) of basalt, dacite, and silica synthetic melt glasses at 65ºC. Based on these data, it was found that the logarithm of glass dissolution rates is linearly related to the wt.% SiO$_2$ in glass. The data of Mazer (1987) were used to extrapolate glass dissolution rates to the SiO$_2$ composition of rhylolitic nuclear melt glass typically found at the NTS (77 wt.% SiO$_2$). It is believed that this glass dissolution rate constant is well known.

In the term accounting for temperature effects on dissolution (known as the Arrhenius factor), only the activation energy, $E_a$, is a fitted constant. Activation energies range typically from 10 to 20 kcal mol$^{-1}$. While the choice of activation energy does not drastically affect the dissolution rate of glass at tempartures close to the reference temperature ($T_0$, typically 25ºC), the effect is dramatic at temperatures far from the

reference temperature. For example, at 150ºC, the range of 10–20 kcal/mol results in a >2 order of magnitude range in dissolution rates; at 50ºC, the same range of activation energies results in a <1 order of magnitude range in dissolution rates (Figure 1).[2] In the simulations of Pawloski et al. (2001), an activation energy of 20 kcal mol$^{-1}$ was used.
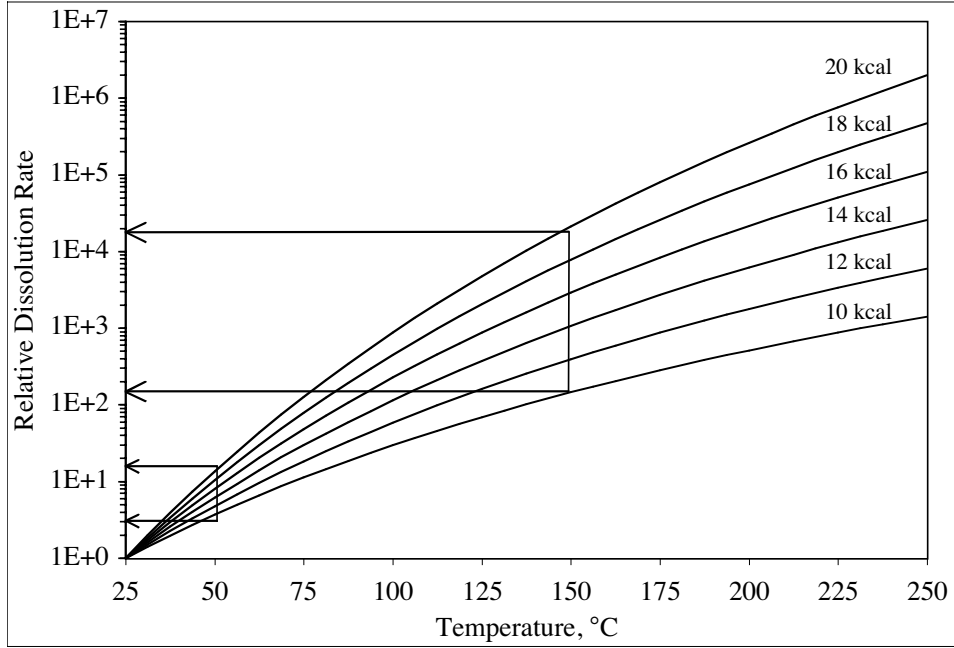


**Figure 1. The effect of activation energy on dissolution rates as a function of temperature.**

The rate of glass dissolution is linearly related to the reactive surface area, $A_s$, of the glass. The surface area of nuclear melt glasses was previously examined and estimated at 0.001 to 0.01 m$^2$/g (Bourcier et al., 2000). Often, the effect of surface area on glass dissolution rate, $r$, is removed by dividing the rate by the reactive surface area:

$$r^* = \frac{r}{A_s} \qquad (2)$$

where $r^*$ is in units of mol m$^{-2}$ sec$^{-1}$. In the following discussion, we use $r^*$ when discussing the glass dissolution rates.

The series of dissolution-inhibiting or dissolution-promoting solution aqueous species activities, $a_i$, with exponents, $n_i$, can include a large number of components. However, the principal species that are used to account for solution composition effects on glass dissolution are H$^+$ and OH$^-$. These two species act to promote dissolution at

---

[2] Based on the assumption that the reference temperature is 25ºC.

3

high and low pH. A plot of the effect of $H^+$ and $OH^-$ on glass dissolution as a function of pH and temperature for the dacite of Mazer (1987) is shown in Figure 2. Two subtle effects should be noted. First, the minimum in the rate decreases in pH with increasing temperature. This occurs because the pH of neutrality decreases with increasing temperature. Second, the pH range over which the neutral term of the dissolution rate equation controls the glass dissolution rate narrows with increasing temperature. In fact, the role of the neutral term becomes insignificant at high temperatures; this effect results from the increasing disproportionation of water at higher temperatures, which increases the role of the $H^+$ and $OH^-$ terms of the dissolution rate equation.
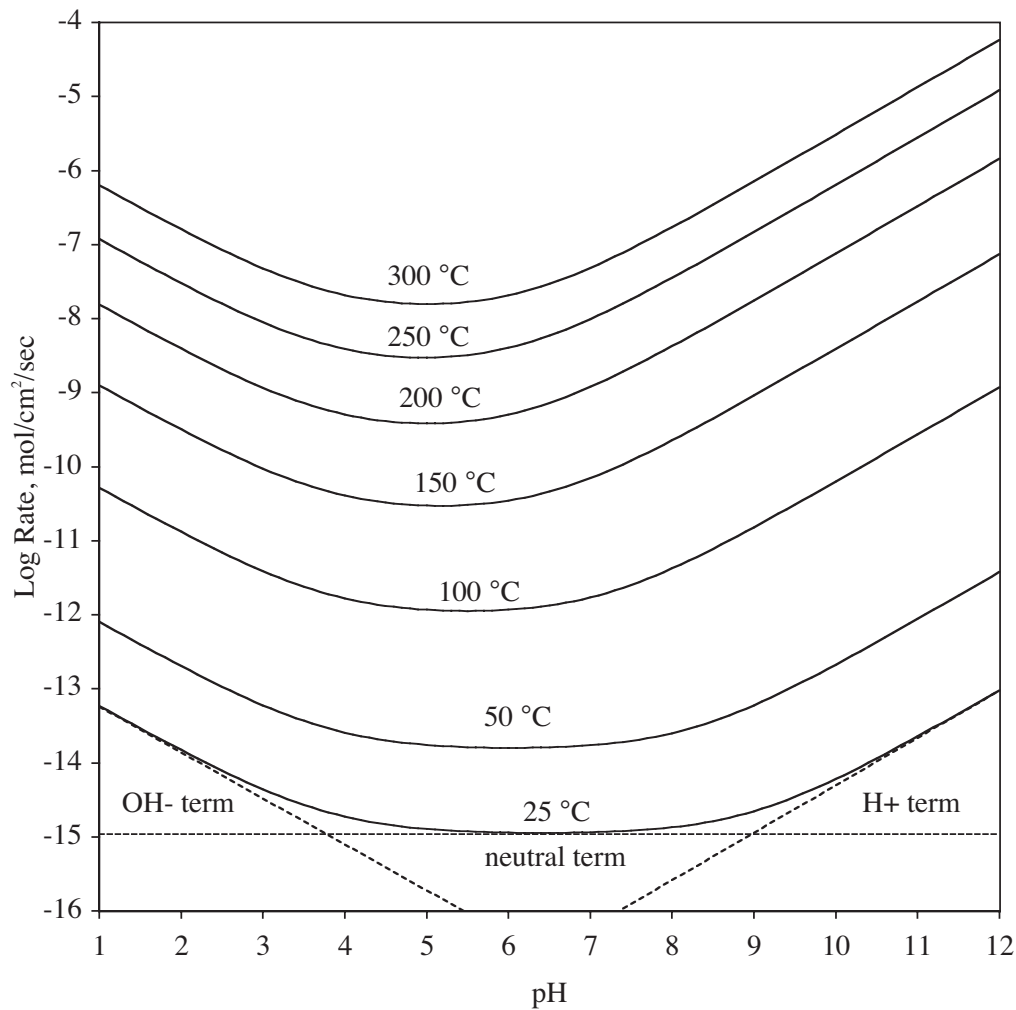


**Figure 2. Effects of temperature and pH on dacite dissolution based on data of Mazer (1987) and activation energy of 20 kcal mol$^{-1}$.**

It should be noted that $H^+$ and $OH^-$ are not the only terms reported to have dissolution-promoting or dissolution-inhibiting effects. An element often reported in the literature to have a significant inhibitory effect on the dissolution of a variety of

aluminosilicate minerals and glasses is Al. The aluminum inhibition exponent at pH 2 and 150ºC for kaolinite ($n_i$) was estimated at –1. For albite at pH 9 and 150ºC, the exponent $n_i$ was estimated at –0.33 (Oelkers et al., 1994). The potential effect of aluminum inhibition will be discussed later in this report.

The saturation term, $1–Q/K$, along with its exponents, $\sigma$ and $\upsilon$, is a complicated term with a number of empirically fitted parameters. For glasses, the term $K$ has been defined by the solubility product of amorphous silica while $Q$ was defined as the activity of $SiO_2(aq)$ (Pawloski et al., 2001). As such, the saturation state of the solution ($Q/K$) is assumed to be controlled entirely by the activity of $SiO_2(aq)$ in solution. This may not necessarily be the case but is assumed to be a reasonable approximation in this report. The effect of the two exponential terms, $\sigma$ and $\upsilon$, is quite different and is shown in Figures 3 and 4. The effect of the $1/\sigma$ term is to reduce the glass dissolution rate drastically even when the solution is relatively undersaturated.[3] In fact, as $\sigma$ is increased, it appears that the shape of the glass dissolution rate as a function of saturation state does not change but is simply shifted to a lower dissolution rate. This is in contrast to the $\upsilon$ term (Figure 4), which tends not to significantly affect the dissolution rate far from saturation but greatly reduces the dissolution rate as saturation is approached.[4] Under ambient solution conditions at the NTS where the saturation term, $1–Q/K$, is equal to 0.7, the $\upsilon$ term is less likely to significantly reduce glass dissolution rates than the $1/\sigma$ term. Later in this report, we evaluate both these terms with regards to fitting our glass dissolution experiment data.

The saturation term, $k_f$, provides a means to continue the dissolution of glass even if saturation with respect to amorphous silica has been reached. This term accounts for the fact that glass is inherently unstable and will continue to dissolve to form more stable precipitates even under saturated conditions.[5] The close-to-saturation rate is, however, typically orders of magnitude lower than the far-from-saturation rate. Thus, the saturation rate affects the rate of glass dissolution only under conditions of high saturation. As will be discussed later in this report, glass dissolution in our experiments was slow enough such that an approach to high saturation was not achieved. Thus, this close-to-saturation term has not been measured. The rate of dissolution slows quickly enough at intermediate levels of saturation such that an approach to saturation is difficult to achieve.

---

[3] Boucier et al. (1994) reported that the $1/\sigma$ for their glass dissolution experiments was 0.1.

[4] For calcite, this term has been reported to be approximately 3 (Bourcier et al., 1994).

[5] Note that saturation is defined based on amorphous silica solubility.
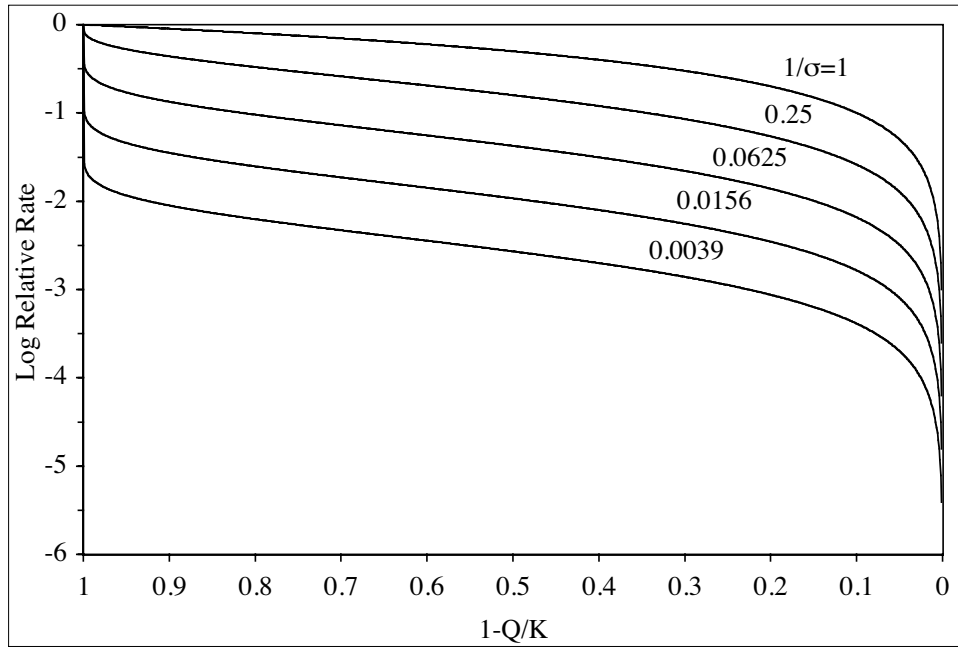
**Figure 3. Effect of $1/\sigma$ on the glass dissolution rate as a function of saturation state.**
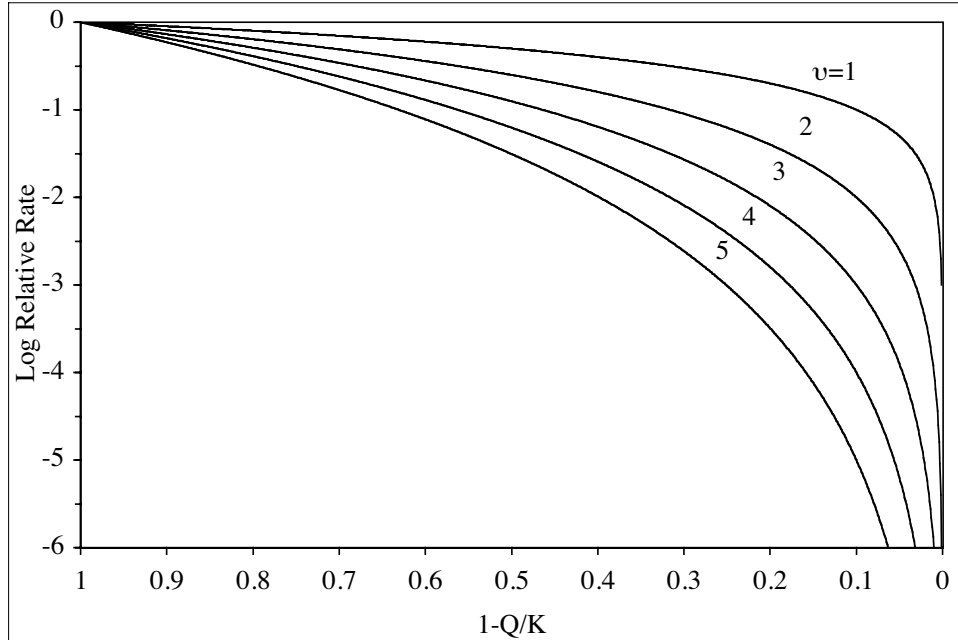


**Figure 4. Effect of $\upsilon$ on the glass dissolution rate as a function of saturation state.**

6

# 3    METHODS

## 3.1    Glass Preparation

3.1.1    Analog Glass

Two glasses were prepared for "near saturation" single-pass flow-through (SPFT) experiments: a Mo-free Lake County Obsidian (LCO) and a LCO doped with $MoO_3$. One-weight-percent $MoO_3$ was used to minimize the potential for Mo to affect the dissolution rate behavior of the glass while maximizing the potential to detect Mo at low glass dissolution rates.  The technique has been used successfully to measure rates of dissolution of extremely slowly reacting ceramics.  The preparation method for each glass is described below, and an electron probe analysis of the Mo-doped and Mo-free LCO glass is given in Table 1.

For the Mo-free LCO glass, approximately 450 g of LCO was placed in a single large platinum crucible and fused in air at 1400ºC for 24 hours.  At the end of the fusion, the furnace temperature was adjusted to 750ºC, and the sample was annealed for 164 hours at that temperature.

For the Mo-doped LCO glass, approximately 450 g of LCO was fused for 2 hours at 1200ºC to dehydrate the sample prior to addition of $MoO_3$.  The dehydrated glass was then run through a tungsten carbide shatterbox and passed through a 125-µm sieve. $MoO_3$ was then added to aliquots of the sample in an amount calculated to yield 1 wt.% $MoO_3$ in the final product.  All of the aliquots were then put in a polyethylene bottle and mixed by hand.  The mixture was then placed in a single large platinum crucible and the sample fused in air at 1400ºC for 24 hours.  The furnace was then cooled to 1000ºC, the sample removed from the furnace and quenched in water.  Examination in transmitted light did not reveal any remaining un-dissolved $MoO_3$ or other crystalline phases.  The resulting Mo-doped glass was then crushed, sieved and fused 2 more times.  The second fusion was for 24 hours, the third for 66 hours.  At the end of the third fusion, the sample was quenched in water and then returned to the furnace at 750ºC for 246 hours to anneal. The water quench cracked the glass, facilitating removal from the crucible.

An aliquot of each sample was mounted in epoxy for electron probe analysis.  The samples were analyzed at 15 kV, with a beam current of 10 nA and a beam diameter of 10 µm.  The analytical precision of a single $MoO_3$ analysis is ~5%.  The average $MoO_3$ content for 30 point analyses of the Mo-doped LCO is 0.91 wt.% with a standard deviation of 0.05 (Table 1).  As such, the sample is homogeneous at the $2\sigma$ level, and further crushing-fusion cycles are unlikely to significantly improve sample homogeneity. The low analytical totals suggest that the sample was slightly damaged by the electron beam.  No $MoO_3$ was detected in the Mo-free LCO.

After preparation, the glasses were crushed, sieved, rinsed repeatedly in alcohol and distilled water, and the 25–53 µm grain size collected for the SPFT tests.

Table 1.  Percent oxide composition of Mo-doped Lake County Obsidian (LCO) glass, and pre-reactor Mo-free LCO glass (based on microprobe analyses).

| Oxide | Mo-doped LCO | Mo-free LCO |
|---|---|---|
| $SiO_2$ | 74.05 | 76.01 |
| $Al_2O_3$ | 12.67 | 13.00 |
| FeO | 0.75 | 0.70 |
| MnO | 0.07 | 0.08 |
| MgO | 0.11 | 0.09 |
| CaO | 0.83 | 0.52 |
| $Na_2O$ | 2.95 | 3.65 |
| $K_2O$ | 4.32 | 4.81 |
| $MoO_3$ | 0.91 | -- |
| $TiO_2$ | -- | 0.11 |
| **Total** | **96.66** | **98.97** |

## 3.1.2   Nuclear Melt Glass

The nuclear melt glass sample (JMK-1) used in the experiments is from an undisclosed underground test that was detonated below the water table on Pahute Mesa. The sample consists of highly vesicular, colorless- to gray-banded glass, similar in appearance to pumice.  Archival drill cuttings of pre-shot volcanic tuff were also obtained from the working point of the same test.  The tuff was expected to have a bulk chemical composition similar to the melt glass (compositional similarity was later confirmed, Table 2), and could therefore be used in the pre-reactor cell of the dissolution apparatus. The volcanic tuff was crushed to –150 mesh size (<0.1 mm), melted at 1450°C in air, and then quenched to produce a homogeneous, non-radioactive "pre-reactor glass."

The major element compositions of the nuclear melt glass and pre-reactor glass samples were analyzed on a JEOL 8200 electron microprobe using a 7.5-nA, 15-keV electron beam defocused to a diameter of 30 μm.  X-ray intensities were converted to element concentrations using a CITZAF algorithm.  Reference standards included a variety of silicate and oxide minerals.  Each sample was analyzed at 10 randomly selected spots.  Compositional averages are reported in Table 2 as oxide weight percent. The results show that the melt glass and pre-reactor glass samples have very similar major element compositions.  Hence, the pre-reactor glass is well suited for producing a solution that is close to chemical equilibrium with the melt glass sample.  The data indicate that the working point lithology for this test was a high-silica rhyolite.

Table 2. Percent oxide composition of JMK-1 melt glass and PM-X pre-reactor glass (based on microprobe analyses).

| Oxide | JMK-1 | PM-X |
|:---:|:---:|:---:|
| | Weight percent | |
| $SiO_2$ | 77.25 | 77.63 |
| $TiO_2$ | 0.07 | 0.08 |
| $Al_2O_3$ | 12.56 | 12.52 |
| FeO | 0.79 | 0.66 |
| MnO | 0.00 | 0.02 |
| MgO | 0.08 | 0.02 |
| CaO | 0.61 | 0.73 |
| $Na_2O$ | 3.25 | 3.59 |
| $K_2O$ | 5.22 | 4.73 |
| **Total** | **99.83** | **99.98** |

Activities and concentrations of gamma-emitting radionuclides were measured in the melt glass sample using a fixed Ge(Li) detector. The total count time was 1 day. Gamma spectra were obtained for $^{60}Co$, $^{137}Cs$, $^{152}Eu$, $^{154}Eu$, $^{155}Eu$, and $^{241}Am$ (Table 3), and reported values reflect activities at the time of data acquisition (31 January 2002). The data reveal that the melt glass is from one of the more recent NTS underground tests (probably <20 years old) as indicated by the readily detectable amounts of fission products with half-lives on the order of 5 to 10 years.

The glass samples were crushed and sieved to obtain particle sizes of 25–53 μm (melt glass) and 25–74 μm (pre-reactor glass). Particles with diameters of <25 μm were removed from the sieved material by washing the glass in water followed by acetone.

Table 3. Gamma spectroscopy results for JMK-1 melt glass sample.

| Isotope | Half-life (years) | Concentration (atoms/g) | γ-activity (dpm/g) |
|:---:|:---:|:---:|:---:|
| $^{60}Co$ | 5.27 | $3.3 \times 10^9$ | $8.3 \times 10^2$ |
| $^{137}Cs$ | 30.2 | $1.7 \times 10^{12}$ | $7.4 \times 10^4$ |
| $^{152}Eu$ | 13.5 | $2.1 \times 10^{10}$ | $2.1 \times 10^3$ |
| $^{154}Eu$ | 8.59 | $3.9 \times 10^9$ | $5.9 \times 10^2$ |
| $^{155}Eu$ | 4.71 | $1.3 \times 10^9$ | $3.7 \times 10^2$ |
| $^{241}Am$ | 433 | $1.9 \times 10^{12}$ | $5.7 \times 10^3$ |

3.1.3    Surface Area Analysis

The surface area of the glasses was measured by BET (Brunauer et al., 1938) using a Micromeritics Gemini II 2370 surface area analyzer.  Results are listed in Table 4.  All samples were outgassed at 110°C; nitrogen gas was used to outgas the non-radioactive samples, and JMK-1 melt glass was outgassed under vacuum.

Importantly, the glass surface areas reported in Table 4 cannot be compared to whole-rock effective reactive surface area measurements reported by Bourcier et al. (2000) or the specific surface area measurements of Papelis et al. (2000) because they do not reflect the surface areas of pristine non-crushed natural glasses.  Glass samples listed in Table 4 were prepared by crushing and sieving the glass (25–53 or 25–74 μm particles) to provide a uniform glass particle size.  The specific surface area of these samples approaches the expected surface area based on non-porous smooth spheres within the sieved particle size range (0.1 to 0.03 m$^2$/g).[6]  However, it is slightly higher than the expected surface area due to entrainement of smaller particles, as can be seen in SEM photos taken of the nuclear melt glass (Zavarin et al., 2004).

Table 4.  Results of surface area analysis for glasses used in dissolution experiments.

| Sample name/number | Surface area (m$^2$/g) |
|---|---|
| Mo-doped-LCO glass | 0.1901 |
| LCO pre-reactor glass | 0.1972 |
| JMK-1 melt glass | 0.2969 |
| PM-X pre-reactor glass | 0.2329 |

## 3.2    Buffer Solution Composition

All SPFT tests were performed using 1mM  NaHCO$_3$ flow through solution.  The pH of the starting solution was ~8.5.  This solution is similar in composition to the low-sodium carbonate waters found at NTS.  In certain analog flow-through experiments, SiO$_2$(aq) was added to the flow-through solutions to increase the saturation state with respect to amorphous silica.  In those cases, the SiO$_2$(aq) concentration in solution was ~100 mg/L, the NaHCO$_3$ concentration was 1 mM, and some nitric acid was used to adjust the pH to 8.5.

---

[6] Papelis et al. (2000) noted that surface areas of material with particles sizes near 10 μm approached the expected surface area based on non-porous smooth spheres in their analog glass samples.

## 3.3    Flow-Through Experiments

### 3.3.1    Analog Glass

Three sets of flow-through experiments to measure glass dissolution rates were performed (40ºC, 60ºC, and 80ºC).  The experimental system consisted of various components that allowed filtered (0.2 μm) solutions to flow through cells containing glass and exit into leachate receivers (Figure 5).  Flow rate and pH could be fixed and monitored as a function of time, and their effects on glass dissolution could be observed and quantified from analysis of leachate.  Gentle rocking during sampling kept the glasses suspended, and allowed the system to behave as a continuously stirred reactor. To ensure that solutions in the flow-through cell approached saturation with respect to silica, a pre-reactor cell was placed in line before the flow-through cell.  This pre-reactor consisted of a large flow-through cell that was packed with crushed glass.  A debubbler cell, which allows gas (primarily $CO_2[g]$) to exsolve during heating and escape, was placed in-line for each experiment.  The experimental system (except the HPLC pump) was placed in an oven to regulate the temperature.  Temperature was monitored by a thermocouple.
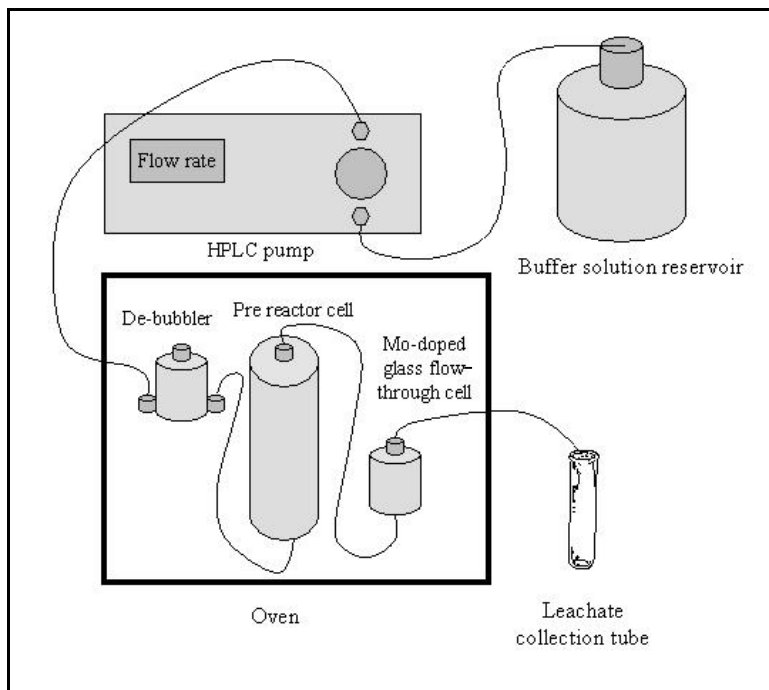


**Figure 5.  Schematic of experimental set-up showing buffer solution reservoir, HPLC pump, flow-through cells in oven, and leachate collection tube.**

A schematic of the experimental set-up is shown in Figure 5, and a photograph of the debubbler and flow-through cells in the oven is shown in Figure 6. At each temperature (40ºC, 60ºC, and 80ºC), solution flow rates of 0.01 mL/min, 0.1 mL/min, and 1.0 mL/min were used. The pore volume of the system was determined by calculating the volumes of the tubing and the reactor cells. We assumed that dissolution of the glass was close to steady state at time of sampling because at each flow rate, an amount equal to several pore volumes of solution was flowed through the cells before leachate samples were collected for analysis. Also, at each flow rate and temperature, several samples were taken to ensure that a steady state had been reached.

Leachate was collected, acidified, and analyzed by ICP-MS for molybdenum, and on ICP-AES for aluminum, calcium, potassium, magnesium, sodium, and silica. All analytical results are listed in Appendices 1–3. The pH was also measured; the pH varied only slightly during these experiments.



**Figure 6. Glass dissolution experimental set-up showing flow-through cell attached to shaker arm at right, pre-reactor cell at left and bubbler cell at upper left.**

### 3.3.2 Nuclear Melt Glass

Nuclear melt glass dissolution experiments were run using a two-cell flow-through reactor similar to that used in analog glass dissolution experiments. The pre-reactor cell is used to raise the silica concentration in solution to near saturation before introducing the solution to the nuclear melt glass. This approach approximates natural fluid conditions expected near the melt glass of underground nuclear tests. A dilute (1 mM) sodium bicarbonate solution was passed through the cells at a rate of ~14 to 16 mL/day, and at temperatures of 40ºC, 60ºC, or 80°C.

The key technical challenge in the nuclear melt glass experiments was to identify a unique trace element or isotope present *only* in the melt glass that could be used to monitor dissolution rates. Using a pre-reactor glass that was compositionally very similar to the melt glass was advantageous in terms of simulating natural dissolution conditions. However, since both samples were from the same source rock, both had nearly identical trace element abundances. This effectively limited the choice of monitoring species to test-derived radionuclides. $^{137}$Cs is present at fairly high concentrations in the melt glass (Table 3), but preliminary leaching rate estimates indicated that the concentration going into solution would be too low to detect by gamma counting. Moreover, the $^{137}$Cs could not be measured on a magnetic sector ICP-MS because of a strong isobaric interference with $^{137}$Ba. After careful consideration of all the options, it was determined that uranium isotopes (in particular, $^{238}$U/$^{235}$U ratios) were the best choice for a dissolution monitor. This decision was guided in part by our ability to accurately measure extremely low uranium abundances (less than 1 part per trillion) on the magnetic sector ICP-MS. In addition, uranium tends to be conservative in aqueous bicarbonate solutions due to its tendency to form soluble uranyl carbonate complexes under slightly alkaline pH conditions (e.g. Langmuir, 1978). However, this choice still depended upon whether the $^{238}$U/$^{235}$U ratio in the melt glass was sufficiently different from the natural abundance in the pre-reactor glass, so that the melt glass uranium contribution could be reliably detected at very low levels in solution.

Small (0.3 g) samples of melt glass and pre-reactor glass were each dissolved in strong $HNO_3$, HF, and $HClO_4$, evaporated to dryness, and then brought back into solution in dilute $HNO_3$. These samples were then analyzed by ICP-MS to determine their uranium concentrations and isotope ratios. The results are given in Table 5. The uranium concentrations in both glasses are similar, but their $^{238}$U/$^{235}$U ratios are quite distinct. Whereas the pre-reactor glass has a natural uranium isotope ratio, the melt glass shows a strong enrichment in $^{235}$U from the nuclear test. Hence, monitoring variations in dissolved $^{238}$U/$^{235}$U ratios during the experiments could provide a means of estimating glass dissolution rates.

Table 5. Uranium concentrations and isotope ratios in JMK-1 and PM-X glass samples.

| Sample | U (ppb) | $^{238}U/^{235}U$ |
|--------|---------|-------------------|
| JMK-1 melt glass | $4637.4 \pm 8.8$ | 14.14 |
| PM-X Pre-reactor glass | $4447.8 \pm 9.0$ | 136.97 |

### 3.3.2.1 Uranium mixing ratios

The uranium concentration and isotope ratio in the solution exiting the flow through reactor represents a mixture of uranium dissolved from the pre-reactor glass and the nuclear melt glass. The relative proportions of uranium from these two sources can be determined by standard isotope dilution calculations (Moore et al., 1973), which are summarized in Faure (1986).

Let $N$ = the number of atoms of natural uranium (from the pre-reactor glass), $S$ = the number of atoms of "spike" uranium (from the nuclear melt glass), and $R_m$ = the measured $^{238}U/^{235}U$ ratio of the mixture. For our experiment, we can write the expression:

$$R_m = \frac{0.9928N + 0.93395S}{0.0072N + 0.06605S} \qquad (3)$$

where: $0.9928$ = the natural $^{238}U$ abundance in the pre-reactor glass
$0.93395$ = the $^{238}U$ abundance in the melt glass
$0.0072$ = the natural $^{235}U$ abundance in the pre-reactor glass, and
$0.06605$ = the $^{235}U$ abundance in the melt glass.

Next we convert to weights of $N$ and $S$ by dividing by Avogadro's number (A) and multiplying by the respective atomic weights of uranium in each glass

$$N_w = 238.0291*N/A \qquad (4)$$

$$S_w = 237.8522*S/A \qquad (5)$$

where $N_w$ = the weight of uranium in the pre-reactor glass, and $S_w$ = the weight of uranium in the melt glass. It follows that the measured weight of the mixture ($W_m$) is defined as

$$W_m = N_w + S_w \qquad (6)$$

Solving (2) and (3) for $N$ and $S$, respectively, substituting these expressions into equation (1), and solving for $N_w$ yields the following equation

$$N_w = S_w\left[\frac{238.0291}{237.8522}\right]\left[\frac{0.93395 - R_m(0.06605)}{R_m(0.0072) - 0.9928}\right] = S_w Q \qquad (7)$$

Next we substitute $S_w = W_m - N_w$ into equation (5) to obtain the final expression for $N_w$

$$N_w = (W_m - N_w)[Q]$$
$$N_w + N_w[Q] = W_m[Q]$$
$$N_w(1 + [Q]) = W_m[Q]$$

$$N_w = \frac{W_m[Q]}{(1 + [Q])} \qquad (8)$$

In practice, $W_m$ and $R_m$ represents the U concentration and $^{238}U/^{235}U$ ratio of the flow through reactor solution, measured by the magnetic sector ICP-MS. The relative proportion of the total U concentration from the pre-reactor glass ($N_w$) and the melt glass ($S_w$) are then calculated from equations (6) and (4), respectively. These data can then be used to calculate glass dissolution rates.

### 3.4    Static Analog Glass Dissolution Experiments

Due to temperature limitations of the SPFT cells, a static, higher temperature experiment was performed at 160ºC in a titanium Parr-bomb apparatus. Ten grams of the Mo-doped glass was reacted with 100 mL of 1 mM $NaHCO_3$ in a Parr-bomb apparatus equipped with a sampling port. Solutions from this static experiment were sampled daily over a period of a week and analyzed for the same elements as the flow-through experiments. Each sampling took ~10 mL solution from the reactor; the first 5 mL were discarded to ensure that the sampling port was flushed of old solution.

### 4    RESULTS AND DISCUSSION

### 4.1    Analog Glass Dissolution

Raw data for the SPFT analog glass dissolution experiments are listed in Appendices 1, 2, and 3. Data from the 160ºC static dissolution experiment are listed in Appendix 4.

Glass dissolution rates were calculated based on Mo concentrations in the fluid exiting the flow-through cells. The following equation was used:

$$r^* = [Mo] \times \frac{mol_{glass}}{mol_{Mo}} \times g_{Mo-glass}^{-1} \times \left( \frac{m^2}{g_{Mo-glass}} \right)^{-1} \times \frac{mL}{min.} \times \frac{0.001L}{mL} \times \frac{1\,min.}{60\,sec} \quad (9)$$

Based on the electron microprobe data, the ratio of mol glass to mol Mo is 153. For all flow-through experiments, the same mass of Mo-glass (1.8057 g) and surface area (0.1901 m$^2$/g) was used. Thus, the rate of glass dissolution could be calculated simply by multiplying the flow rate and the concentration of Mo (mol/L) by $7.43 \times 10^{-3}$. Based on these calculations, average dissolution rates were calculated for each temperature and flow condition. The results are listed in Table 6. Standard deviations are quite small indicating that reaction rates reached steady state in all experiments.

For the 160ºC Parr bomb experiments, rates were based on the change in Mo concentration between sampling time intervals in the following manner:

$$r^* = \frac{[Mo]_2 - [Mo]_1}{t_2 - t_1} \times \frac{mol_{glass}}{mol_{Mo}} \times g_{Mo-glass}^{-1} \times \left( \frac{m^2}{g_{Mo-glass}} \right) \times Vol._1 \quad (10)$$

where $t$ is in seconds and *Vol.* is the volume of solution in the Parr bomb over that particular time interval (liters). The rates are reported in Table 6 together with the flow-through experiments.

Also included in Table 6 is the pH of solutions corrected for temperature. These temperatures were calculated based on the pHs reported at 25ºC. The equivalent pH at temperature was calculated using the geochemical modeling code Geochemist's Workbench (Bethke, 1998) and GEMBOCHS database version V8.R6 (Johnson and Lundeen, 1997).

Table 6. Average rates of glass dissolution based on data reported in Appendices 1–4.

| Temp ºC | Time (days) | Flow Rate (mL/min) | pH at T | Si (log mol/L) | Rate (log mol glass m$^{-2}$ sec$^{-1}$) |
|---|---|---|---|---|---|
| 40 | - | 0.01 | 7.80 | -3.55(0.04) | -12.19(0.04) |
| 40 | - | 0.1 | 8.19 | -4.08(0.04) | -11.55(0.06) |
| 40 | - | 0.1 | 8.06 | -2.77(0.01) | -12.00(0.04) |
| 40 | - | 1.0 | 8.05 | -6.09(0.10) | -11.24(0.04) |
| 60 | - | 0.01 | 7.76 | -3.08(0.01) | -11.48(0.12) |
| 60 | - | 0.1 | 7.89 | -3.46(0.01) | -10.89(0.03 |
| 60 | - | 0.1 | 7.89 | -2.75(0.01) | -11.45(0.07) |
| 60 | - | 1.0 | 8.03 | -4.35(0.02) | -11.20(0.05) |
| 80 | - | 0.01 | 7.87 | -2.88(0.03) | -11.39(0.09) |
| 80 | - | 0.1 | 7.89 | -3.11(0.01) | -10.75(0.06) |
| 80 | - | 0.1 | 7.85 | -2.73(0.00) | -11.55(0.06) |
| 80 | - | 1.0 | 7.76 | -3.57(0.04) | -10.31(0.14) |
| 160 | 0.92 | 0 | 7.60 | -2.66 | -8.99 |
| 160 | 1.78 | 0 | 7.61 | -2.55 | -9.60 |
| 160 | 2.91 | 0 | 7.61 | -2.48 | -9.79 |
| 160 | 4.10 | 0 | 7.56 | -2.40 | -9.96 |
| 160 | 4.97 | 0 | 7.69 | -2.34 | -9.75 |
| 160 | 5.91 | 0 | 7.69 | -2.31 | -10.27 |
| 160 | 6.86 | 0 | 7.70 | -2.29 | -10.23 |

## 4.2    Nuclear Melt Glass Dissolution

Data from the JMK-1 melt glass dissolution experiments are listed in Appendices 5, 6, and 7. Appendix 5 summarizes the sampling chronology during the melt glass dissolution experiments and the corresponding reactor flow rates (in mL/day). Sample IDs that begin with 'RGL' indicate fluids that passed through both the pre-reactor and the melt glass reactor; samples designated 'PGL' passed through only the pre-reactor, and did not interact with the melt glass.

Appendix 6 contains the results of magnetic sector ICP-MS analyses of Si and U concentrations and $^{238}$U/$^{235}$U ratios in the reactor solutions. The table also includes calculated values for the relative fraction of U dissolved from the pre-reactor and melt glass ($N_w$ and $S_w$, respectively). As anticipated, the measured $^{238}$U/$^{235}$U ratios of the pre-reactor solutions ('PGL') are all very close to the natural ratio (137.88), and this ratio has been used in the calculations. In contrast, the solution exiting the melt glass reactor ('RGL') had measured $^{238}$U/$^{235}$U ratios ranging from 97.1 to 70.0. Despite the difference in isotopic ratios, there is generally no significant difference in the measured U concentrations of the 'PGL' and 'RGL' samples at a given reaction temperature (Appendix 6). Thus, the isotope data clearly indicate that uranium from the melt glass is going into solution, while the concentration data show that the net contribution from the melt glass is small—which is consistent with near-saturated conditions. This relationship is quantified by the values for $N_w$, $S_w$, and $Q$ in Appendix 6, where $Q = N_w/S_w$. These

data show that the fraction of dissolved U from the melt glass comprises only 5 to 12% of the total amount of U in solution.  The measured Si concentrations exhibit variations at each reaction temperature.  Both Si and U show distinct increases in their average concentrations with temperature, which reflect enhanced glass dissolution rates at higher temperatures.

Appendix 7 reports the calculated glass dissolution rates for the melt glass samples.  A summary of the relevant data is presented in Table 7.  The dissolution rates for the nuclear melt glass were based on the U isotope data.  For the 60ºC rate data, a standard deviation could not be estimated because only two data points were reported.  Since pH was not measured, the pH, corrected for temperature, was estimated based on the pHs measured for the analog glass experiments.

Table 7.  Average rates of glass dissolution based on data reported in Appendix 7.

| Temp ºC | Flow Rate (mL/min) | pH at T | Si (log mol/L) | Rate (log mol glass $m^{-2}$ $sec^{-1}$) |
|---|---|---|---|---|
| 40 | 0.009 | 7.80 | -3.52(0.08) | -11.66(0.08) |
| 60 | 0.009 | 7.76 | -3.28(0.11) | -11.14(?)* |
| 80 | 0.010 | 7.87 | -2.86(0.09) | -10.77(0.02) |

* Standard deviation could not be calculated.

## 4.3    Modeling Glass Dissolution

The data reported in Tables 6 and 7 can be compared to the predicted glass dissolution rates based on the TST model (Equation 1).  To properly evaluate these data, the saturation state of these solutions with respect to the analog and nuclear melt glass needs to be known.  The saturation state ($Q/K$) of the solutions was based on the activity of aqueous $SiO_2(aq)$ and the solubility of amorphous silica from the GEMBOCHS database (Johnson and Lundeen, 1997).  We plot all the data in Figure 7 with the $1-Q/K$ term along the x-axis and the log dissolution rate on the y-axis.

Along with the data, we have plotted two sets of predicted glass dissolution rate functions.  The first is based on the model used in recent Cheshire HST simulations (Pawloski et al., 2001) and the second is based on a TST model with adjusted parameters.  In the CHESHIRE model (Pawloski et al., 2001), the $s$ and $u$ terms and the close-to-saturation term were ignored.  The activation energy was set to 20 kcal/mol, $Q$ was set by the aqueous activity of $SiO_2(aq)$, K was set by the solubility of amorphous $SiO_2$, and the rate constant and affinity terms were of the following form:

$$k_0 \times \prod_i a_i^{n_i} \approx 10^{-11.59} + 10^{-8.01} \times \left(OH^-\right)^{0.5155} + 10^{-9.51} \times \left(H^+\right)^{0.4566} \qquad (11)$$

In the modified model, the close-to-saturation term was ignored while the $\sigma$ term was set to 100 ($\upsilon$ term not used). The activation energy was set to 12 kcal/mol, the $Q$ and $K$ terms

18

were treated as before, and the rate constant and affinity terms were of the following form:[7]

$$k_0 \times \prod_i a_i^{n_i} \approx 10^{-11.33} + 10^{-8.28} \times \left(OH^-\right)^{0.5519} + 10^{-9.24} \times \left(H^+\right)^{0.4825} \qquad (12)$$

Justification for the modified model will be given below.

### 4.3.1 General Trends in Glass Dissolution Data

The following observations can be made based on the set of collected experimental data:

- At all temperatures, the dissolution rates tend to decrease with $1–Q/K$, with approximately a 1-order-of-magnitude variation between the least saturated and most saturated sample.

- The dissolution rates based on the nuclear melt glass are consistent with the analog glass results, suggesting that the two glasses behave similarly.

- Rates increase drastically with temperature.

It should be noted that all analog flow-through data were calculated by assuming that background Mo concentrations were negligible.[8] While this is a reasonable assumption in most cases, it may result in an overestimate of the glass dissolution rate in certain cases. For example, at $1–Q/K = 0.38$ and at 40ºC, background Mo accounts for nearly 75% of the Mo in solution. The high background is the result of the very slow dissolution rates of the Mo-doped glass under these conditions. In general, when Mo concentrations approach 0.1 ppb, the fraction of background Mo in the effluent becomes significant. To err on the side of conservative glass dissolution rates, background subtraction was not employed in any of the glass dissolution rate calculations.

Another factor to acknowledge is that at high flow rates (1.0 mL/min.), it cannot be assumed that flowing fluids access the entire volume of glass. It may be possible that preferential flow in the columns at these flow rates would artificially reduce the apparent glass dissolution rates. This is likely to be the case in the 60ºC low saturation data which resulted in glass dissolution rates apparently slower than the data at higher saturation.

---

[7] The rate constant and affinity terms differ slightly from the original unclassified model of Pawloski et al. (2001) due to subtle improvements to the original data fitting. However, this effect is rather minor.

[8] Trace concentrations of Mo are pervasive in the laboratory, resulting in high background Mo concentrations in all solutions used in the laboratory.

4.3.2    Comparing Glass Dissolution Data to Model Predictions

Predicted glass dissolution rates based on the TST model recently used in
CHESHIRE simulations (Pawloski et al., 2001) are presented in Figure 7 (thin dashed
lines).  Comparison of these model predictions with experimental data suggests that the
glass dissolution model used in CHESHIRE simulations was quite conservative.  The most
dramatic difference between predicted and experimental dissolution rates appears to
occur at the higher temperatures, suggesting that the activation energy used in the
CHESHIRE near-field model was high (20 kcal/mol).  Yokohama and Banfield (2002)
recently measured the dissolution rates of rhyolite glass from Japan at relatively low
aqueous silica concentrations.  Based on 50ºC, 30ºC, and 15ºC data, they estimated an
activation energy of 15 kcal/mol.  As shown in Figure 1, this reduced activation energy
would result in an order of magnitude decrease in predicted glass dissolution rates at
160°C.  While this does not reduce the predicted glass dissolution rate enough to arrive at
a good model fit to the experimental data, it brings the predicted and experimental data
closed together.

Because measured glass dissolution rates appear to be significantly lower than
predicted rates even under relatively unsaturated conditions, the TST model parameter
that would best account for the observed behavior is the stoichiometric number σ (See
Figure 3 and compare with Figure 4).  Predicted glass dissolution rates based on adjusted
σ parameter and activation energy are presented in Figure 7 (thick lines).  The TST
model was adjusted in the following manner:

- Activation energy was reduced from 20 kcal/mol to 12 kcal/mol.[9]

- The stoichiometric number was employed with a value of 100.

While the fit is only approximate, and relatively conservative for the 160ºC data,
the model is significantly more consistent with the data than the earlier CHESHIRE glass
model.  Furthermore, it is interesting to note that, when using this adjusted model, the
predicted dissolution rates compare well with the values reported by Yokohama and
Banfield (2002) for 15ºC, 30ºC, and 50ºC glass dissolution ($2.1\times10^{-17}$, $8.2\times10^{-17}$, and
$4.1\times10^{-16}$ versus $3.5\times10^{-17}$, $8.7\times10^{-17}$, and $6.1\times10^{-16}$ mol/m$^2$/sec, respectively).  This
provides additional evidence that the adjusted glass dissolution model can predict glass
dissolution rates reasonably well.

Some additional discussion of the source of the high stoichiometry number is
relevant.  While this value improves the fit to the data, this stoichiometry number is too
high to have a realistic physical significance.[10]  A σ of 100 suggests, in fact, that our TST

---

[9] An activation energy of 12 kcal/mol was used instead of 15 kcal/mol to arrive at a better
model fit.
[10] Bourcier et al. (1994) reported that σ = 10 fit their data on dissolution of waste glasses
at 100ºC.

model may not be accounting for other processes that may slow glass dissolution. One likely reaction that has not been accounted for by our model is the potential for dissolution inhibition by aqueous Al. Oelkers et al. (1994) suggested that aqueous Al may be a prominent inhibitor of aluminosilicate dissolution. Published experimental data suggest an inhibition value of $[Al]^{-1}$ for kaolinite and $[Al]^{-0.33}$ for albite. In Figure 8, we present the predicted glass dissolution rate at 40ºC based on the CHESHIRE model, based on $\sigma = 100$, and based on $\sigma = 1$ (i.e. no exponent) and an Al inhibition function consistent with that observed by Oelkers et al. (1994) for albite. Clearly, the reduced dissolution rates observed in our experiments may result from the inhibitory nature of Al on the glass surface.[11] It is also interesting to note that the inhibitory nature of Al (based on congruent dissolution of the glass) cannot be distinguished from the effect of the stoichiometry number, $\sigma$. Based on these results, it appears that either an Al inhibition model or a high stoichiometry number could be used to bring the glass dissolution model used in near-field HST simulations closer to the experimentally observed glass dissolution rates.

---

[11] Note that, if the values based on the data of kaolinite were used, the inhibition would be significantly more severe.
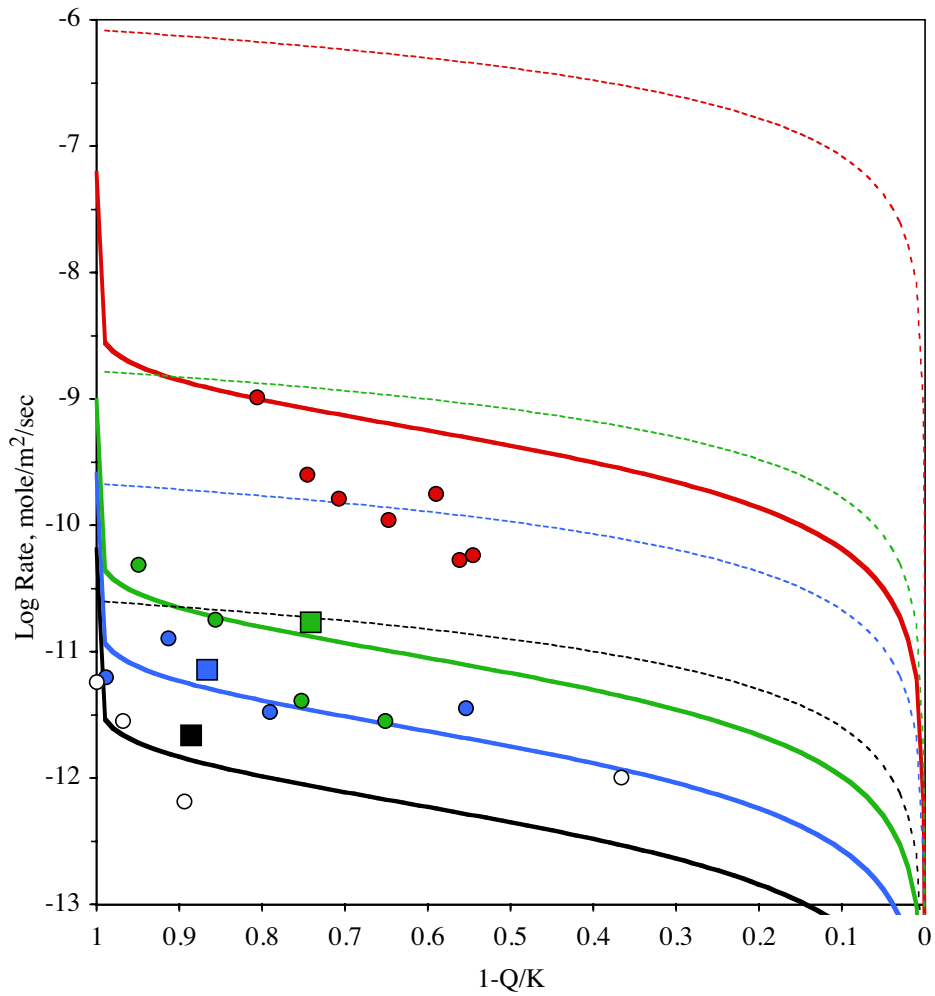
**Figure 7. Comparison of predicted to measured glass dissolution rates. Predicted rates based on the glass dissolution rate equation used in Pawloski et al. (2001) (thin dashed lines), and rates based on the adjusted glass dissolution rate model (thick lines). Nuclear melt glass data (squares) and analog glass data (circles). T=40ºC (black), T=60ºC (blue), T=80ºC (green), and T=160ºC (red).**
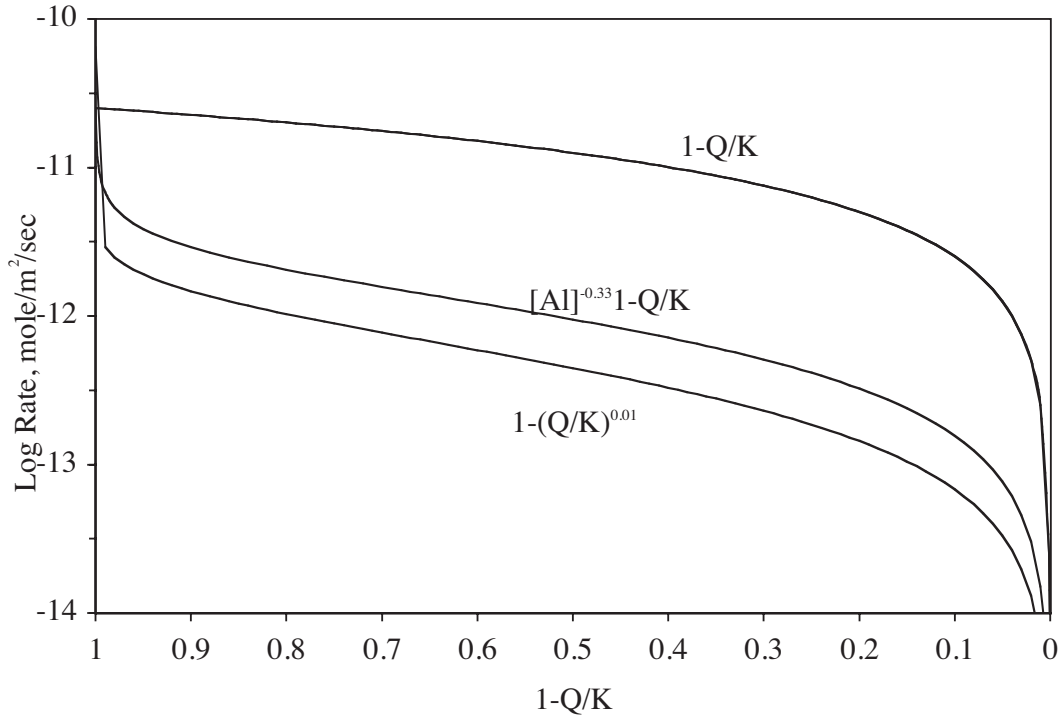
**Figure 8. The effect of Al inhibition on glass dissolution rate as a function of saturation state at 40ºC.**

## 5   CONCLUSIONS AND RECOMMENDATIONS

Based on the reported experimental data:

- Dissolution rates of analog and nuclear melt glasses are equivalent.

- It appears that glass dissolution rates in recent HST simulations (Pawloski et al., 2001; Wolfsberg et al., 2001) were too fast, particularly at high temperatures.

- In future simulations, the activation energy for glass should be reduced from 20 kcal/mol to between 15 and 12 kcal/mol.

- Glass dissolution appears to slow down at even low saturation levels. The effect of solution saturation on glass dissolution can be modeled either with a high stoichiometry number ($\sigma = 100$) or by accounting for the likely inhibition of glass dissolution by aqueous Al.

With regard to the fourth point listed above, the most appropriate method by which to account for the reduced glass dissolution rates as a function of solution saturation needs further examination. While the role of Al in inhibiting the dissolution of aluminosilicates has been widely observed, it is not yet clear how glass dissolution and secondary mineral precipitation will be affected in the complex and heterogeneous glass zone of a nuclear test cavity.

23

## 6 ACKNOWLEDGEMENTS

## 7 REFERENCES

Bethke, C. M. (1998) The Geochemist's Workbench: Release 3.0. University of Illinois.

Bourcier, W.L., Carroll, S.A., and Phillips, B.L. (1994) Constraints on the affinity term for modeling long-term glass dissolution rates. Materials Research Society Symposium Proceedings, 333: 507-512.

Bourcier, W.L., Roberts, S.K., Newton, L., Sawvel, A., Bruton, C. (2000) Part 2. Determination of reactive surface areas from flow-through test of natural analog glass samples *In* Determination of Reactive Surface Area of Melt Glass, Bourcier, W. Roberts, S., Smith, D.K., Hulsey, S., Newton, L., Sawverl, A., Bruton, C., Papelis, C., Um, W., Russel, C.E., and Chapman, J., UCRL-ID-145181, Lawrence Livermore National Laboratory, Livermore, California.

Brunauer, S., Emmet, P.H., and Teller, E. (1938) Adsorption of gases in multimolecular layers. Journal American Chemican Society, 60: 309-318.

Faure, G. (1986) Principles of Isotope Geology, Second Edition. Wiley, New York, 589 p.

Johnson J. W. and Lundeen S. R. (1997) GEMBOCHS thermodynamic datafiles for use with the EQ3/6 modeling package. Internal Report, Lawrence Livermore National Laboratory, Livermore, California.

Jorgensen, S.S. (1968) Solubility and dissolution kinetics of precipitated amorphous silica in 1 M $NaClO_4$ at 25$^o$C. Acta Chemica Scandinavica, 22, 335-341.

Langmuir, D. (1978) Uranium solution-mineral equilibria at low temperatures with applications to sedimentary ore deposits. Geochimica et Cosmochimica Acta, 42: 547-569.

Mazer, J.J. (1987) Kinetics of glass dissolution as a function of temperature, glass composition, and solution pH's. Ph.D. thesis, Northwestern University.

Moore, L.J., Moody, J.R., Barnes, I.L., Gramich, J.W., Murphy, T.J., Paulsen, P.J., and Shields, W.R. (1973) Trace determination of rubidium and strontium in silicate glass standard reference materials. Analytical Chemistry, 45: 2384-2387.

Oelkers, E.H., Schott, J., and Devidal, J-L. (1994) The effect of aluminum, pH, and chemical affinity on the rates of aluminum dissolution reactions. Geochimica et Cosmochimica Acta, 58: 2011-2024.

Papelis, C., Um, W., Russell, C.E., and Chapman, J.B. (2000) Measuring the specific surface area of natural and man-made glasses. Effect of formation process, morphology, and particle size. *In* Determination of Reactive Surface Area of Melt Glass, Bourcier, W. Roberts, S., Smith, D.K., Hulsey, S., Newton, L., Sawverl, A., Bruton, C., Papelis, C., Um, W., Russel, C.E., and Chapman, J., UCRL-ID-145181, Lawrence Livermore National Laboratory, Livermore, California.

Pawloski G. A., Tompson A. F. B., Bruton C. J., and Zavarin M., Eds. (2000) Evaluation of the Hydrologic Source Term from Underground Nuclear Tests in Frenchman Flat and the Nevada Test Site (U). Contributors: W.L. Bourcier, C.J. Bruton, S.F. Carle, B.K. Esser, A.B. Kersting, R.M. Maxwell, G.A. Pawloski, J.A. Rard, D.E. Shumaker, D.K. Smith, A.F.B. Tompson, and M. Zavarin. UCRL-ID-138007, Lawrence Livermore National Laboratory, Livermore, California.

Pawloski G. A., Tompson A. F. B., and Carle S. F. (2001) Evaluation of the Hydrologic Source Term from Underground Nuclear Tests on Pahute Mesa at the Nevada Test Site: The CHESHIRE Test, Bourcier, W.L., Bruton, C.J., Carle, S.F., Daniels, J.I., Maxwell, R.M., Pawloski, G.A., Shumaker, D.S., Smith, D.K., Tompson, A.F.B., and Zavarin, M., Contributors. UCRL-ID-147023, Lawrence Livermore National Laboratory, Livermore, California.

Tompson A. F. B., Bruton C. J., and Pawloski G. A. (1999) Evaluation of the hydrologic source term from the underground nuclear tests in Frenchman Flat and the Nevada Test Site: The CAMBRIC test. UCRL-ID-132300, Lawrence Livermore National Laboratory, Livermore, California.

Wolfsberg, A. Glascoe, L., Lu, G., Olson, A., Lichtner, P. McGraw, M., Cherry, T., Roemer, G. 2002. Tybo/Benham: Model Analysis of Groundwater Flow and Radionuclide Migration from Undergrounds Nuclear Tests in Southwestern Pahute Mesa, Nevada, LA-13977, Los Alamos National Laboratory, Los Alamos, New Mexico.

Yokoyama, T., and Banfield, J.F. (2002) Direct determinations of the rates of rhyolite dissolution and clay formation over 52,000 years and comparison with laboratory measurements. Geochim. Cosmochim. Acta, 66, No.15, 2665-2681.

Zavarin, M., Roberts, S.K., Viani, B.E., Pawloski, G.A., and Rose, T.P. (2004) Nuclear Melt Glass Dissolution and Secondary Mineral Precipitation at 40 to 200ºC, UCRL-TR-204870, Lawrence Livermore National Laboratory, Livermore, California.

# APPENDIX 1.  ANALYTICAL DATA FROM THE MO-DOPED GLASS STATIC DISSOLUTION EXPERIMENT AT 40ºC

**Mo-doped glass SPFT Experiment #5**
**Mass of Mo-doped glass = 1.8057 grams**

**Buffer solution of 0.001 Molar NaHCO₃**
**Mass of pre-reactor LCO glass = 68.59 grams**

| Sample # | Collection Time hrs | Solution mass g | pH | Flow-Rate mL/min | Mo ppb | Al ppm | Ca ppm | K ppm* | Mg ppm | Na ppm | Si ppm |
|---|---|---|---|---|---|---|---|---|---|---|---|
| **0.01 mL/min** | | | | | | | | | | | |
| Mo#5-1 | 17.20 | 10.127 | 7.91 | 0.010 | 1.24 | 0.97 | 0.03 | n.d. | 0.02 | 24 | 9.0 |
| Mo#5-2 | 16.90 | 9.714 | 7.76 | 0.010 | 1.03 | 0.80 | 1.10 | 0.17 | 0.02 | 24 | 7.8 |
| Mo#5-3 | 16.85 | 9.903 | 8.24 | 0.010 | 1.14 | 0.87 | 1.20 | 0.38 | 0.02 | 24 | 7.5 |
| Mo#5-4 | 17.67 | 10.631 | 7.67 | 0.010 | 1.26 | 0.88 | 1.20 | 2.2 | 0.02 | 24 | 7.5 |
| PR#5-1 | 15.73 | 9.320 | 8.43 | 0.010 | 0.49 | 0.89 | 1.10 | n.d. | 0.02 | 24 | 7.3 |
| **0.1 mL/min** | | | | | | | | | | | |
| Mo#5-5 | 2.30 | 13.420 | 8.50 | 0.097 | 0.47 | 0.57 | 1.20 | 0.71 | 0.03 | 24 | 2.5 |
| Mo#5-6 | 1.67 | 9.756 | 8.10 | 0.098 | 0.49 | 0.45 | 1.20 | n.d. | 0.03 | 23 | 2.6 |
| Mo#5-7 | 1.67 | 9.885 | 8.35 | 0.099 | 0.43 | 0.38 | 2.10 | 0.96 | 0.03 | 23 | 2.2 |
| Mo#5-8 | 2.20 | 13.061 | 8.22 | 0.099 | 0.53 | 0.32 | 1.20 | n.d. | 0.03 | 24 | 2.1 |
| Mo#5-9 | 2.05 | 12.206 | 8.45 | 0.099 | 0.62 | 0.45 | 1.60 | n.d. | 0.03 | 23 | 2.4 |
| PR#5-2 | 1.87 | 11.303 | 7.94 | 0.101 | 0.13 | 0.38 | 1.10 | 0.22 | 0.02 | 23 | 1.7 |
| **Switched solution to 0.001 NaHCO₃, 100 ppm SiO₂** | | | | | | | | | | | |
| Mo#5-10 | 2.22 | 12.903 | 8.37 | 0.097 | 0.19 | 0.21 | 1.30 | n.d. | 0.05 | 96 | 47 |
| Mo#5-11 | 2.40 | 13.887 | 8.08 | 0.096 | 0.19 | 0.20 | 1.10 | n.d. | 0.04 | 96 | 47 |
| Mo#5-12 | 2.02 | 11.627 | 8.15 | 0.096 | 0.18 | 0.02 | 1.20 | n.d. | 0.03 | 96 | 48 |
| Mo#5-13 | 1.65 | 10.038 | 8.17 | 0.101 | 0.16 | 0.10 | 1.20 | n.d. | 0.02 | 97 | 48 |
| Mo#5-14 | 2.32 | 13.409 | 8.14 | 0.096 | 0.16 | 0.22 | 1.10 | 0.97 | 0.02 | 97 | 48 |
| PR#5-3 | 1.03 | 6.164 | 8.00 | 0.099 | 0.14 | 0.15 | 2.50 | n.d. | 0.03 | 98 | 48 |
| **1.0 mL/min** | | | | | | | | | | | |
| **Switched solution to 0.001 NaHCO₃** | | | | | | | | | | | |
| Mo#5-15 | 0.20 | 11.799 | 8.21 | 0.983 | 0.35 | 0.15 | 1.90 | 0.26 | 0.02 | 23 | 0.7 |
| Mo#5-16 | 0.22 | 12.761 | 8.11 | 0.982 | 0.10 | 0.08 | 0.95 | n.d. | 0.01 | 23 | 0.02 |
| Mo#5-17 | 0.24 | 14.551 | 8.11 | 1.004 | 0.11 | 0.10 | 1.20 | n.d. | 0.01 | 23 | 0.02 |
| Mo#5-18 | 0.20 | 11.792 | 8.25 | 0.983 | 0.09 | 0.15 | 0.87 | n.d. | 0.01 | 23 | 0.03 |
| PR#5-4 | 0.22 | 12.930 | 8.15 | 0.995 | 0.08 | 0.13 | 1.10 | 1.6 | 0.02 | 23 | 0.05 |
| 1M NaHCO₃-1 | | | | | 0.05 | 0.11 | 1.00 | n.d. | 0.01 | 23 | n.d. |
| 1M NaHCO₃-2 | | | | | 0.05 | 0.04 | 0.93 | n.d. | 0.01 | 23 | n.d. |
| 100 ppm SiO₂-1 | | | | | | | | | | | 48 |
| 101 ppm SiO₂-2 | | | | | | | | | | | 47 |

*n.d.* = below detection limit

# APPENDIX 2. ANALYTICAL DATA FROM THE MO-DOPED GLASS STATIC DISSOLUTION EXPERIMENT AT 60°C

**Mo-doped glass SPFT Experiment #3**
**Mass of Mo-doped glass = 1.8057 grams**

**Buffer solution of 0.001 Molar NaHCO₃**
**Mass of pre-reactor LCO glass = 68.59 grams**

| Sample # | Collection Time hrs | Solution mass g | pH | Flow-Rate mL/min | Mo ppb | Al ppm | Ca ppm | K ppm* | Mg ppm | Na ppm | Si ppm |
|---|---|---|---|---|---|---|---|---|---|---|---|
| **0.01 mL/min** | | | | | | | | | | | |
| Mo#3-1 | 10.48 | 6.183 | 8.06 | 0.010 | 8.49 | 3.755 | 0.591 | 1.694 | 0.007 | 31.90 | 24.37 |
| Mo#3-2 | 14.72 | 9.347 | 7.93 | 0.011 | 6.33 | 3.716 | 0.682 | 1.322 | 0.007 | 31.24 | 23.22 |
| Mo#3-3 | 13.48 | 8.152 | 7.85 | 0.010 | 5.32 | 3.997 | 0.584 | 1.094 | 0.006 | 30.94 | 23.20 |
| Mo#3-4 | 22.72 | 13.865 | 7.91 | 0.010 | 4.42 | 4.051 | 0.569 | 0.988 | 0.006 | 30.91 | 22.96 |
| PR#3-2 | 16.72 | n.m. | n.m. | n.m. | 0.20 | 3.914 | 0.682 | 0.931 | 0.009 | 30.92 | 21.85 |
| **0.1 mL/min** | | | | | | | | | | | |
| Mo#3-5 | 2.02 | 11.738 | 8.11 | 0.097 | 2.05 | 1.817 | 1.333 | 0.635 | 0.029 | 25.22 | 9.30 |
| Mo#3-6 | 2.17 | 12.688 | 8.17 | 0.098 | 2.44 | 1.803 | 0.657 | 2.453 | 0.008 | 26.01 | 9.73 |
| Mo#3-7 | 2.45 | 14.195 | 8.07 | 0.097 | 2.23 | 1.836 | 0.804 | 2.336 | 0.011 | 25.86 | 9.77 |
| Mo#3-8 | 2.17 | 12.803 | 8.16 | 0.098 | 2.39 | 1.824 | 0.837 | 2.193 | 0.047 | 24.89 | 9.78 |
| Mo#3-9 | 1.33 | 7.819 | 8.10 | 0.098 | 2.28 | 1.840 | 1.017 | 1.739 | 0.053 | 24.38 | 9.86 |
| PR#3-3 | 0.52 | n.m. | n.m. | n.m. | 0.31 | 1.982 | 0.692 | 1.229 | 0.038 | 28.46 | 11.13 |
| **Switched solution to 0.001 NaHCO₃, 100 ppm SiO₂** | | | | | | | | | | | |
| Mo#3-9a | 1.85 | 10.415 | 8.05 | 0.094 | 0.82 | 0.321 | 0.961 | 2.329 | 0.074 | 84.52 | 49.24 |
| Mo#3-10 | 2.22 | 12.565 | 8.03 | 0.094 | 0.65 | 0.296 | 1.098 | 1.848 | 0.058 | 84.68 | 50.88 |
| Mo#3-11 | 2.02 | 11.435 | 8.22 | 0.095 | 0.60 | 0.221 | 0.883 | 1.023 | 0.033 | 84.86 | 49.54 |
| Mo#3-12 | 2.58 | 15.090 | n.m. | 0.097 | 0.56 | 0.254 | 0.891 | 1.208 | 0.026 | 86.14 | 49.50 |
| Mo#3-13 | 1.77 | 10.225 | 8.18 | 0.096 | 0.57 | 0.185 | 0.837 | 1.007 | 0.020 | 87.63 | 50.52 |
| PR#3-4 | 0.98 | n.m. | n.m. | n.m. | 0.24 | 0.201 | 0.798 | 0.313 | 0.021 | 86.90 | 51.00 |
| **1.0 mL/min** | | | | | | | | | | | |
| Mo#3-14 | 0.18 | 10.963 | 8.28 | 0.997 | 0.10 | 0.322 | 0.611 | -0.610 | 0.003 | 19.64 | 1.33 |
| **Switched solution to 0.001 NaHCO₃** | | | | | | | | | | | |
| Mo#3-15 | n.m. | n.m. | 8.32 | n.m. | 0.11 | 0.236 | 0.815 | -0.426 | 0.005 | 19.76 | 1.26 |
| Mo#3-16 | n.m. | n.m. | 8.32 | n.m. | 0.10 | 0.236 | 0.796 | -0.660 | 0.005 | 19.81 | 1.26 |
| Mo#3-17 | n.m. | n.m. | 8.40 | n.m. | 0.13 | 0.257 | 1.044 | -0.550 | 0.008 | 19.17 | 1.17 |
| PR#3-5 | n.m. | n.m. | n.m. | n.m. | 0.08 | 0.408 | 0.811 | -0.489 | 0.010 | 20.66 | 2.90 |
| 1M NaHCO₃-1 | | | | | 0.07 | 0.020 | 0.589 | -0.451 | 0.009 | 23.41 | 0.22 |
| 100 ppm SiO₂ | | | | | 0.03 | 0.000 | 0.749 | -0.545 | 0.005 | 82.97 | 48.69 |

*n.m.* = not measured

* Potassium analyses suspect due to detection limits

# APPENDIX 3. ANALYTICAL DATA FROM THE MO-DOPED GLASS STATIC DISSOLUTION EXPERIMENT AT 80°C

**Mo-doped glass SPFT Experiment #4**  
**Mass of Mo-doped glass = 1.8057 grams**

**Buffer solution of 0.001 Molar NaHCO₃**  
**Mass of pre-reactor LCO glass = 68.59 grams**

| Sample # | Collection Time hrs | Solution mass g | pH | Flow-Rate mL/min | Mo ppb | Al ppm | Ca ppm | K ppm* | Mg ppm | Na ppm | Si ppm |
|---|---|---|---|---|---|---|---|---|---|---|---|
| **0.01 mL/min** | | | | | | | | | | | |
| Mo#4-1 | 15.32 | 9.812 | 8.46 | 0.011 | 7.97 | 6.75 | 0.93 | 1.06 | 0.01 | 34.71 | 38.01 |
| Mo#4-2 | 16.48 | 10.287 | 8.23 | 0.010 | 8.81 | 6.66 | 0.73 | 1.11 | 0.01 | 35.87 | 37.85 |
| Mo#4-3 | 14.27 | 8.346 | 8.27 | 0.010 | - | 7.47 | 0.83 | 1.05 | 0.01 | 41.13 | 41.12 |
| Mo#4-4 | 16.12 | 9.488 | 8.38 | 0.010 | 5.90 | 7.55 | 0.83 | 1.09 | 0.02 | 38.54 | 40.57 |
| Mo#4-5 | 17.37 | 11.777 | 8.18 | 0.011 | 5.73 | 6.20 | 0.79 | 0.98 | 0.01 | 33.20 | 34.47 |
| Mo#4-6 | 16.73 | 10.407 | 8.25 | 0.010 | 8.66 | 6.63 | 0.83 | 1.14 | 0.01 | 33.65 | 36.48 |
| PR#4-2 | 19.25 | 12.040 | 8.70 | 0.010 | 0.89 | 6.83 | 0.74 | 2.12 | 0.01 | 34.05 | 37.39 |
| **0.1 mL/min** | | | | | | | | | | | |
| Mo#4-8 | 1.78 | 11.372 | 8.33 | 0.106 | 3.51 | 3.93 | 0.76 | 1.05 | 0.01 | 27.35 | 21.18 |
| Mo#4-9 | 1.75 | 10.745 | 8.30 | 0.102 | 3.64 | 4.19 | 1.03 | 1.01 | 0.06 | 27.17 | 21.69 |
| Mo#4-10 | 1.63 | 10.056 | 8.40 | 0.103 | 2.99 | 4.08 | 0.92 | 1.03 | 0.09 | 26.74 | 21.98 |
| Mo#4-11 | 1.60 | 9.645 | 8.34 | 0.100 | 2.72 | 4.05 | 0.91 | 1.20 | 0.09 | 26.42 | 21.82 |
| PR#4-3 | 1.57 | 9.267 | 8.29 | 0.099 | 0.41 | 4.01 | 0.92 | 2.33 | 0.09 | 26.47 | 21.49 |
| **Switched solution to 0.001 NaHCO₃, 100 ppm SiO₂** | | | | | | | | | | | |
| Mo#4-12 | 1.82 | 9.582 | 8.36 | 0.088 | 0.62 | 1.07 | 1.04 | 3.11 | 0.08 | 101.64 | 53.27 |
| Mo#4-13 | 1.68 | 10.206 | 8.33 | 0.101 | 0.45 | 0.96 | 0.95 | 2.64 | 0.06 | 99.35 | 52.30 |
| Mo#4-14 | 1.73 | 10.830 | 8.23 | 0.104 | 0.48 | 0.95 | 0.88 | 2.67 | 0.05 | 101.30 | 52.50 |
| Mo#4-15 | 1.62 | 10.301 | 8.19 | 0.106 | 0.52 | 0.80 | 1.18 | 2.70 | 0.05 | 101.07 | 52.39 |
| Mo#4-16 | 1.62 | 9.990 | 8.19 | 0.103 | 0.47 | 0.82 | 1.25 | 2.62 | 0.05 | 101.30 | 52.83 |
| PR#4-4 | 1.80 | 10.403 | 8.24 | 0.096 | 0.09 | 0.93 | 0.93 | 2.93 | 0.05 | 100.12 | 52.37 |
| **Switched solution to 0.001 NaHCO₃** | | | | | | | | | | | |
| **1.0 mL/min** | | | | | | | | | | | |
| Mo#4-17 | 0.20 | 12.330 | 8.16 | 1.028 | 0.57 | 1.54 | 0.60 | 0.67 | 0.01 | 24.96 | 6.75 |
| Mo#4-18 | 0.18 | 11.361 | 8.03 | 1.033 | 0.67 | 1.58 | 0.97 | 0.79 | 0.01 | 25.50 | 7.20 |
| Mo#4-19 | 0.20 | 11.258 | 8.06 | 0.938 | 1.00 | 1.50 | 0.95 | 0.86 | 0.01 | 25.43 | 8.10 |
| Mo#4-20 | 0.20 | 11.567 | 8.03 | 0.964 | 1.12 | 1.60 | 0.88 | 0.91 | 0.01 | 25.58 | 7.96 |
| Mo#4-21 | 0.18 | 11.490 | 8.01 | 1.045 | 1.16 | 1.53 | 0.86 | 0.76 | 0.01 | 25.02 | 8.09 |
| PR#4-5 | 0.18 | 11.171 | 8.00 | 1.016 | 0.16 | 1.65 | 0.85 | 1.01 | 0.01 | 24.41 | 8.38 |
| 1M NaHCO₃-1 | | | | | 0.00 | - | - | - | - | - | - |
| 1M NaHCO₃-2 | | | | | 0.00 | - | - | - | - | - | - |
| 100 ppm SiO₂ | | | | | 0.03 | - | - | - | - | - | - |

\* Potassium analyses suspect due to detection limits

# APPENDIX 4.  ANALYTICAL DATA FROM THE MO-DOPED GLASS STATIC DISSOLUTION EXPERIMENT AT 160°C

**Mo-doped glass static dissolution Experiment #1**
**Mass of Mo-doped glass = 9.6498 grams**
**Volume of 0.001 Molar NaHCO$_3$ buffer solution = 100 mL**

**Start date**     9/4/02 3:30 PM

| Sample # | Sample date | Elapsed time days | pH | Psi | Mo ppb | Al ppm | Ca ppm | K ppm | Mg ppm | Na ppm | Si ppm |
|---|---|---|---|---|---|---|---|---|---|---|---|
| | | 0.00 | 8.03 | | | | | | | | |
| PB1-1 | 9/5/02 1:30 PM | 0.92 | 8.07 | 86 | 1338 | 9.5 | 2.4 | 3.1 | 0.22 | 39 | 61 |
| PB1-2 | 9/6/02 10:19 AM | 1.78 | 8.08 | 82 | 1684 | 12.7 | 1.4 | 5.9 | 0.15 | 42 | 80 |
| PB1-3 | 9/7/02 1:15 PM | 2.91 | 8.17 | 79 | 2008 | 15.4 | 1.2 | 5.2 | 0.12 | 45 | 92 |
| PB1-4 | 9/8/02 5:51 PM | 4.10 | 7.74 | 79 | 2274 | 18.8 | 1.2 | 4.0 | 0.09 | 47 | 111 |
| PB1-5 | 9/9/02 2:43 PM | 4.97 | 8.80 | 78 | 2639 | 21.4 | 1.2 | 4.4 | 0.07 | 52 | 129 |
| PB1-6 | 9/10/02 1:25 PM | 5.91 | 8.80 | 76 | 2782 | 22.7 | 1.1 | 5.0 | 0.06 | 55 | 138 |
| PB1-7 | 9/11/02 12:15 PM | 6.86 | 8.86 | 75 | 2979 | 23.4 | 1.3 | 4.8 | 0.06 | 56 | 143 |
| PB1-8 | 9/12/02 12:19 PM | 7.87 | 7.09 | 72 | 2013 | 14.2 | 2.0 | 3.5 | 0.13 | 40 | 94 |
| PB1-9 | 9/13/02 8:55 AM | 8.73 | 7.04 | 70 | 1033 | 7.2 | 1.6 | 2.3 | 0.10 | 25 | 54 |

# APPENDIX 5. ANALYTICAL DATA FROM THE JMK-1 MELT GLASS SPFT EXPERIMENT AT 40º, 60º, AND 80ºC

**Melt glass from NTS JMK-1:**         sample mass 1.0801 g, 25-53 mm
**Preshot glass:**         sample mass 14.962 g, 25-74 mm
**Experiment start date:**         6/5/02 11:00 AM

| Sample ID | Temp. | sampling start | sampling end | React time, day | sample mass | Flow rate, mL/day |
|---|---|---|---|---|---|---|
| RGL-40.1-1 | 40.5 | 6/18/02 6:44 PM | 6/19/02 9:06 AM | **13.62** | **7.8675** | **13.14** |
| RGL-40.1-2 | 40.6 | 6/19/02 5:55 PM | 6/20/02 9:17 AM | **14.61** | **8.6580** | **13.52** |
| RGL-40.1-3 | 40.6 | 6/21/02 6:48 PM | 6/22/02 11:01 AM | **16.66** | **9.1276** | **13.51** |
| RGL-40.1-4 | 39.0 | 6/24/02 8:55 AM | 6/24/02 6:24 PM | **19.11** | **5.0981** | **12.90** |
| PGL-40.1-1 | 38.9 | 6/25/02 9:30 AM | 6/25/02 5:42 PM | **20.11** | **4.6402** | **13.58** |
| RGL-40.1-5 | 38.9 | 7/1/02 4:33 PM | 7/2/02 11:16 AM | **26.62** | **10.4014** | **13.34** |
| PGL-40.1-2 | 39.2 | 7/2/02 12:34 PM | 7/2/02 4:17 PM | **27.14** | **2.2323** | **14.41** |
| RGL-40.1-6 | 39.1 | 7/3/02 4:46 PM | 7/8/02 8:01 AM | **30.56** | **62.8939** | **13.57** |
| PGL-40.1-3 | 40.5 | 7/8/02 2:00 PM | 7/8/02 4:38 PM | **33.18** | **1.5152** | **13.81** |
| RGL-40.1-7 | 40.1 | 7/9/02 11:43 AM | 7/10/02 8:03 AM | **34.45** | **11.4293** | **13.49** |
| PGL-40.1-4 | 39.1 | 7/10/02 11:40 AM | 7/10/02 4:33 PM | **35.13** | **2.8695** | **14.10** |
| **Change oven temperature to 60 ºC on:** | | 7/10/02 4:30 PM | | run time from temp. change, day | | |
| test flow rate | 65.0 | 7/11/02 8:00 AM | 7/12/02 7:59 AM | **1.15** | **13.6002** | **13.61** |
| change temp. | 60.6 | 7/12/02 8:00 AM | | | | |
| RGL-60-1 | 60.8 | 7/17/02 4:22 PM | 7/18/02 8:28 AM | **7.33** | **9.0262** | **13.46** |
| PGL-60-1 | 60.7 | 7/18/02 11:47 AM | 7/18/02 4:36 PM | **7.90** | **2.9377** | **14.64** |
| RGL-60-2 | 60.7 | 7/22/02 4:33 PM | 7/23/02 8:27 AM | **12.33** | **8.7529** | **13.21** |
| PGL-60-2 | 60.4 | 7/23/02 4:59 PM | 7/24/02 8:39 AM | **13.35** | **8.6480** | **13.25** |
| RGL-60-3 | 60.5 | 7/30/02 8:37 AM | 7/31/02 8:27 AM | **20.17** | **13.1664** | **13.26** |
| PGL-60-3 | 60.7 | 7/31/02 12:15 PM | 8/1/02 8:20 AM | **21.24** | **12.0953** | **14.45** |
| **Change oven temperature to 80 ºC on:** | | 8/8/2002 10:00 | | | | |
| test | 79.9 | 8/12/2002 10:12 | 8/13/2002 8:23 | **4.47** | **12.5265** | **13.55** |
| test | 79.3 | 8/13/2002 8:25 | 8/19/2002 11:15 | **11.05** | **80.8443** | **13.21** |
| Sample ID | Temp. | sampling start | sampling end | React time, day | sample mass | Flow rate, mL/day |
| RGL-80-1 | 79.3 | 8/19/2002 11:19 | 8/20/2002 8:32 | **11.50** | **11.4155** | **12.91** |
| RGL-80-2 | 79.4 | 8/20/2002 8:32 | 8/21/2002 9:32 | **12.46** | **15.3149** | **14.70** |
| RGL-80-3 | 80.0 | 8/21/2002 9:32 | 8/22/2002 9:30 | **13.48** | **13.8305** | **13.85** |
| PGL-80-1 | 79.9 | 8/22/2002 12:19 | 8/23/2002 8:48 | **14.52** | **13.8422** | **16.22** |
| PGL-80-2 | 80.0 | 9/9/2002 12:39 | 9/10/2002 9:06 | **32.54** | **11.9604** | **14.04** |

# APPENDIX 6. MAGNETIC SECTOR ICP-MS ANALYSES OF SI AND U CONCENTRATIONS AND $^{238}$U/$^{235}$U RATIOS IN JMK-1 REACTOR SOLUTIONS

|  | 238U | 235U | 238/235 | Mixed U Atomic Wt. |
|---|---|---|---|---|
| Atomic Wt. | 238.050785 | 235.043922 |  |  |
| U-Nat atom abundance | 0.9928 | 0.0072 | 137.88 | 238.02914 |
| Melt Glass abundance | 0.93395 | 0.06605 | 14.14 | 237.85218 |

Avogadros No.
6.02214E+23 — Terms defined in text

| Sample ID | $R_m$ 238/235 | 2-S | Atomic Wt. | $W_M$ ppb (U conc) | Q | $N_W$ (Wt of U-Nat) | $S_W$ (Wt of Melt Glass) | Si (ppm) | Uncertainty |
|---|---|---|---|---|---|---|---|---|---|
| RGL-40.1-5 | 97.1040 | 1.0981 | 238.02014 | 0.03449 | 18.67467 | 0.03274 | 0.00175 | 9.58 | 0.48 |
| PGL-40.1-2 | 137.8800 |  | 238.02914 | 0.04146 |  |  |  | 7.45 | 0.37 |
| RGL-40.1-6 | 85.2244 | 0.7283 | 238.01591 | 0.03350 | 12.39138 | 0.03100 | 0.00250 | 8.42 | 0.42 |
| PGL-40.1-3 | 137.8800 |  | 238.02914 | 0.02834 |  |  |  | 6.86 | 0.34 |
| RGL-40.1-7 | 89.4617 | 0.8629 | 238.01755 | 0.03098 | 14.27886 | 0.02895 | 0.00203 | 7.87 | 0.39 |
| PGL-40.1-4 | 137.8800 |  | 238.02914 | 0.03244 |  |  |  | 11.29 | 0.56 |
|  |  |  |  |  |  |  |  |  |  |
| PGL 60-2 | 137.88 |  | 238.02914 | 0.05751 |  |  |  | 16.3 | 0.8 |
| RGL 60-2 | 75.1048 | 0.0904 | 238.01128 | 0.06160 | 8.91441 | 0.05539 | 0.00621 | 19.8 | 1.0 |
| PGL 60-3 | 137.88 |  | 238.02914 | 0.06320 |  |  |  | 11.7 | 0.6 |
| RGL 60-3 | 70.0392 | 0.0698 | 238.00846 | 0.06658 | 7.56346 | 0.05880 | 0.00777 | 12.0 | 0.6 |
|  |  |  |  |  |  |  |  |  |  |
| PGL 80-1 | 137.88 |  | 238.02914 | 0.27899 |  |  |  | 112.9 | 5.6 |
| PGL 80-2 | 137.88 |  | 238.02914 | 0.21840 |  |  |  | 32.6 | 1.6 |
| RGL 80-1 | 80.4768 | 0.0647 | 238.01388 | 0.19141 | 10.60752 | 0.17492 | 0.01649 | 37.9 | 1.9 |
| RGL 80-2 | 82.0878 | 0.0638 | 238.01460 | 0.19637 | 11.17881 | 0.18025 | 0.01612 | 51.6 | 2.6 |
| RGL 80-3 | 84.8508 | 0.0502 | 238.01576 | 0.20178 | 12.23942 | 0.18654 | 0.01524 | 34.6 | 1.7 |

# APPENDIX 7.  CALCULATED GLASS DISSOLUTION FOR THE PM-X PRE-REACTOR AND JMK-1 MELT GLASS SAMPLES

**Sample Properties**

| | Pre-reactor Glass sample | | | | Nuclear Melt Glass sample | | |
|---|---|---|---|---|---|---|---|
| | Starting S.A. (BET) | 0.2329 | $m^2/g$ | | Starting S.A. (BET) | 0.2969 | $m^2/g$ |
| | Glass Density (est.) | 2.6 | $g/cm^3$ | | Glass Density (est.) | 2.6 | $g/cm^3$ |
| | WtFrac Oxide | Element | WtFrac Element | | WtFrac Oxide | Element | WtFrac Element |
| SiO2 | 0.7763 | Si | 0.3629 | SiO2 | 0.7725 | Si | 0.3611 |
| UO3 | 0.27 | U | 4.448E-06 | UO3 | 0.27 | U | 4.637E-06 |

**Pre-Reactor Cell - Si and U Dissolution Rates  (U data from $W_m$ values in Appendix 6)**

| pH 8 | Mass of Pre-Reactor Glass | Flow Rate | Run time from day 1 | Particle Diameter | Surf. Area | Run time from temp. change | | | Glass Dissoln. Rate | Glass Dissoln. Rate |
|---|---|---|---|---|---|---|---|---|---|---|
| | (g) | (mL/day) | (days) | (μm) | (sq. m) | | Si | U | NR-Si | NR-U |
| start | 14.9620 | | 0.00 | 9.909 | 3.48465 | | (ppb) | (ppb) | mol/m^2/sec | mol/m^2/sec |
| PGL-40-2 | 14.9609 | 14.41 | 27.14 | 9.908 | 3.48449 | 27.14 | 7.45E+03 | 0.04146 | 9.83E-12 | 4.462E-12 |
| PGL-40-3 | 14.9607 | 13.81 | 33.18 | 9.908 | 3.48445 | 33.18 | 6.86E+03 | 0.02834 | 8.67E-12 | 2.923E-12 |
| PGL-40-4 | 14.9606 | 14.10 | 35.13 | 9.908 | 3.48444 | 35.13 | 1.13E+04 | 0.03244 | 1.46E-11 | 3.416E-12 |
| PGL-60-2 | 14.9596 | 13.25 | 48.58 | 9.908 | 3.48427 | 13.35 | 1.63E+04 | 0.05751 | 1.98E-11 | 5.691E-12 |
| PGL-60-3 | 14.9591 | 14.45 | 56.47 | 9.908 | 3.48420 | 21.24 | 1.17E+04 | 0.06320 | 1.55E-11 | 6.821E-12 |
| PGL-80-2 | 14.9524 | 14.04 | 96.49 | 9.906 | 3.48316 | 32.54 | 3.26E+04 | 0.21840 | 4.19E-11 | 2.291E-11 |

**Pre-Reactor Cell - U Dissolution Rates (using $N_w$ values from Appendix 6)**

| pH 8 | Mass of Pre-Reactor Glass | Flow Rate | Run time from day 1 | Particle Diameter | Surf. Area | Run time from temp. change | | | Glass Dissoln. Rate | Glass Dissoln. Rate |
|---|---|---|---|---|---|---|---|---|---|---|
| | (g) | (mL/day) | (days) | (μm) | (sq. m) | | Si | U | NR-Si | NR-U |
| start | 14.9620 | | 0.00 | 9.909 | 3.48465 | | (ppb) | (ppb) | mol/m^2/sec | mol/m^2/sec |
| RGL-40-5 | 14.9607 | 14.41 | 26.62 | 9.908 | 3.48444 | 27.14 | 9.58E+03 | 0.03274 | 1.26E-11 | 3.523E-12 |
| RGL-40-6 | 14.9605 | 13.81 | 30.56 | 9.908 | 3.48442 | 33.18 | 8.42E+03 | 0.03111 | 1.06E-11 | 3.209E-12 |
| RGL-40-7 | 14.9603 | 14.10 | 34.45 | 9.908 | 3.48439 | 35.13 | 7.87E+03 | 0.02895 | 1.02E-11 | 3.049E-12 |
| RGL-60-2 | 14.9591 | 13.25 | 47.56 | 9.908 | 3.48420 | 13.35 | 1.98E+04 | 0.05539 | 2.40E-11 | 5.482E-12 |
| RGL-60-3 | 14.9586 | 14.45 | 55.40 | 9.908 | 3.48412 | 21.24 | 1.20E+04 | 0.05880 | 1.59E-11 | 6.346E-12 |
| RGL-80-1 | 14.9541 | 16.22 | 75.46 | 9.907 | 3.48343 | 14.52 | 3.79E+04 | 0.17492 | 5.63E-11 | 2.120E-11 |
| RGL-80-2 | 14.9538 | 16.22 | 76.42 | 9.907 | 3.48338 | 14.52 | 5.16E+04 | 0.18025 | 7.67E-11 | 2.184E-11 |
| RGL-80-3 | 14.9536 | 16.22 | 77.44 | 9.907 | 3.48335 | 14.52 | 3.46E+04 | 0.18654 | 5.14E-11 | 2.261E-11 |

**Melt Glass Reactor Cell - U Dissolution Rates (using $S_w$ values from Appendix 6)**

| pH 8 | Mass of Pre-Reactor Glass (g) | Flow Rate (mL/day) | Run time from day 1 (days) | Diameter (μm) | Surf. Area (sq. m) | Run time from temp. change | Si (est.) (ppb) | | pH at T, estimated | Glass Dissoln. Rate NR-U mol/m^2/sec |
|---|---|---|---|---|---|---|---|---|---|---|
| start | 1.08010 | | 0 | 7.77262 | 0.3207 | | | | | |
| RGL-40-5 | 1.08005 | 13.34 | 26.62 | 7.77252 | 0.3207 | 27.14 | 350 | 7.80 | 1.436E-06 | 1.817E-12 |
| RGL-40-6 | 1.08004 | 13.57 | 30.56 | 7.77248 | 0.3207 | 33.18 | 700 | 7.80 | 2.921E-06 | 2.641E-12 |
| RGL-40-7 | 1.08003 | 13.49 | 34.45 | 7.77246 | 0.3207 | 35.13 | 450 | 7.80 | 1.867E-06 | 2.132E-12 |
| RGL-60-2 | 1.07996 | 13.21 | 47.56 | 7.77228 | 0.3207 | 13.35 | 1200 | 7.76 | 4.874E-06 | 6.386E-12 |
| RGL-60-3 | 1.07989 | 13.36 | 55.4 | 7.77213 | 0.3206 | 21.24 | 1700 | 7.76 | 6.984E-06 | 8.081E-12 |
| RGL-80-1 | 1.07957 | 12.91 | 75.46 | 7.77136 | 0.3206 | 14.52 | 3400 | 7.87 | 1.350E-05 | 1.658E-11 |
| RGL-80-2 | 1.07956 | 14.71 | 76.42 | 7.77132 | 0.3206 | 15.52 | 3400 | 7.87 | 1.538E-05 | 1.847E-11 |
| RGL-80-3 | 1.07954 | 13.85 | 77.44 | 7.77128 | 0.3206 | 16.52 | 3200 | 7.87 | 1.363E-05 | 1.644E-11 |
| % loss | 0.0504 | | | | | | | | | |